THE CFD STUDIES ON THE INFLUENCE OF UN-WETTED AREA ON THE HEAT TRANSFER PERFORMANCE OF THE HORIZONTAL TUBE FALLING FILM EVAPORATION

by

Dilli BALAJI[a*], Ramalingam VELRAJ[b], and Malavarappu RAMANAMURTHY[a]

[a] National Institute of Ocean Technology, Chennai, India
[b] Institute of Energy Studies, Chennai, India

Original scientific paper
https://doi.org/10.2298/TSCI200414056B

This paper discusses about the effect of un-wetted area of tube on the heat transfer performance of horizontal tube falling film evaporation. A 2-D CFD model was developed to perform simulations and investigate the output and validated them with published data available in the literature. In the present study the volume of fluid method is used to track the boundary of the liquid vapour from the contours of volume fraction. Effect of varying tube wall temperature or wall super heat (6-11 °C) on un-wetted area, heat transfer coefficients, and mass transfer coefficients of the circular tube were obtained from the simulation model and the results were analysed and reasons were identified and discussed here. The threshold value of wall super heat above which phase change occurs between liquid film and tube surface is identified as 6 °C. Also it is noted that mass transfer rate increases and then decreases with increase of wall super heat and heat transfer coefficient showed declining trend.

Key words*: un-wetted area, CFD modelling, dry patches, mass transfer rate, heat transfer rate, falling film, wall super heat*

Introduction

As far as falling film evaporation is concerned, several techniques are developed by the researchers for enhancing the falling film evaporation process. In the present work, a CFD model was developed to investigate the issues of un-wetted area or onset of dry out regions on the horizontal tube falling film evaporator tubes performance, which is considered to be one of the main factor that degrades the performance of the falling film evaporation process. Nowaday, CFD plays an important role in the field of heat transfer for investigating the physical and thermal behaviour of the fluids in the heat exchanging process by solving some of the governing equations. In the present paper, some of the literature works on the CFD studies have been discussed in relation the subject of the present work for having a clear idea.

Asbik *et al*. [1] carried out a numerical study of the onset of transverse and longitudinal transitions between turbulent and laminar regimes when the liquid film is evaporated on the horizontal elliptical tube. Effect of gravity, pressure gradients, and viscous forces are considered in the numerical study but not the interfacial shear stress. Turbulence models are preferred for the present study with implicit Keller method to discretize the transfer equations. Influence

* Corresponding author, e-mail: poojkavyam16@gmail.com

of various turbulence models along with parameters like the spray density length, the Froude number, the temperature difference between the wall and the liquid-vapour interface, and the ellipticity, on the transition position are investigated.

Pu *et al*. [2] developed a 2-D numerical model with different tube shapes to simulate heat and mass transfer process using CFD and validated the heat transfer coefficient (HTC) of simulation with an experimental data. Flow and heat transfer characteristics of falling film evaporation on a circular tube and three flat tubes are investigated, respectively. It is confirmed that the liquid film becomes thinner and thinner as height-width ratio increases and average film thickness of three flat tubes is nearly 2.9-16.5% smaller than that of circular tube. Additionally, the cross-sections of flat tube have a lower dimensionless temperature and a thinner thermal boundary-layer, which means a better heat transfer performance compared with the circular tube. The average HTC of three flat tubes is approximately 2.2%, 4.2%, and 11.2% higher than that of the circular tube, respectively.

Zhou *et al.* [3] carried out numerical studies using double-phase coupled heat transfer process in the horizontal-tube falling film evaporation. In this work a method of element sliced out of tube was presented and the continuous double-phase transformation was shown by the discrete mass fraction of steam in the tube. The volume of fluid (VOF) method was applied to investigate the influence of the spray density on the distributions of the film thickness and the circumferential and axial HTC of horizontal-tube. The computation results showed that the circumferential film thickness remains unstable. The thinnest film thickness appeared approximately at the angular positions of 100-140° and dry spot appeared at the bottom of the horizontal-tube. Christians *et al.* [4] conducted experimental studies on different tube configurations such as single tube and also multiple tubes with ten rows in a single column in falling film evaporation process using R-134a and R-236fa refrigerants. As a continuation of an earlier study, they developed techniques to predict the nucleate pool boiling HTC, the onset of un-wetting area as well as bundle heat transfer performance for enhanced boiling tubes.

Tahir *et al.* [5] focuses on CFD works done towards improvising the performance of multi effect distillation (MED) falling film evaporator from the literature. They presented the CFD modelling and methodologies for broadening the operating range of MED plants, scale formation, CO_2 release, uneven liquid distribution along the tube bundle length and uneven vapor flow inside shell and vapour flow in co-current/cross direction. They presented optimized design with higher overall HTC, improved wettability, and less susceptibility to scale formation in the falling film evaporation for MED plants. Esquivel *et al.* [6] claimed that poor liquid distribution the tubes and uncompleted wetting of the tube are the main challenges in the falling film evaporator. The authors suggested a design option based on the height of the feed hole and the geometry of the tube edge. They carried out simulation with CFD using CFX ANSYS 14.0 with multi-phase and free surface models. They worked on the laminar flow regime. A break up was observed in the flow model with rivulet formation, brink depth and counter flow from the air. Numerical study showed that the greatest amount of wetted area on the wall is achieved with variable slope edges at a low distributor plate height.

Wang *et al*. [7], Bohn and Davis [8], and Zhiwei *et al*. [9] performed surface dry out studies for sub-cooled liquid films at convective evaporation conditions and on vertical surfaces. Yang *et al*. [10] carried out numerical studies on the bundles of horizontal tubes based on the distributed parameter method. In the numerical simulation studies, liquid-flow rate and maldistribution on the tube bundles are analysed about their influences on the dry patch formation and heat transfer performance of the evaporator. They observed 12% decrement in the heat transfer capacity as the dry patches reaches around 50% of the heat transfer area of the tube. Less flow

rate of the refrigerant leads to occurance of the more dry patches. As the refrigerant flow rate goes above a certain value, no significant improvement in the heat transfer performance is observed with the flow rate due to dry patches being too small. Li *et al*. [11] carried out numerical studies on the flow characteristics of a liquid film flowing over a smooth surface and structured surface with the Reynolds number range from 10-1121. They used the mixture of R21 and R114 refrigerants in their work. They performed 3-D transient simulations for capturing liquid vapour interface. They focused their studies on the effects of the inlet dimension, inlet flow rates, surface tension, and surface structuring on the wettability, average velocity, and film thickness. They observed that surface tension is important for a good simulation. They also noted that inlet width has no effect on the liquid film evaporation in the steady-state flow regime. For low flow rates, wetting area and film thickness both are little, and developes dry spots.

Most of the literature survey discussed that due to the low Reynolds number and uneven distribution of the liquid film, the dry patches or unwetted area occurs. But the present work discusses about the formation of unwetted area between the liquid film and the tube surface using VOF method. There is a lack of discussion in this area according to the literature survey carried out especially using VOF method. There is a technical gap found in this area, therefore, the present work focused on this area using CFD tool.

Numerical procedure for the present problem

The CFD odelling

A CFD model is developed for investigating a problem. The CFD model of the present problem consists of tubes of 14 mm diameter placed in a single column placed one below another positioned at a 7 mm interval. A sample of CFD model with dimension for 11 mm feeder height is shown in fig. 1. Liquid feeder of varying height is used in this model such as 5 mm, 7 mm, 9 mm, and 11 mm for feeding water on the heat transfer tubes. This CFD model is used for investigating the un-wetted area formation on the tube due to high heat flux at low spray density and also to study the phase change that occurs between liquid film and tube outer surface when the wall super heat goes beyond 6 K. In this CFD model, water from feeder is assumed to be flowing from the top over the heated tubes and thin film of liquid forms on the tube surface under gravity and finally liquid separates from the tube at the bottom. The ANSYS FLUENT 14.0 version is used for the analysis of flow modelling of a falling film liquid.

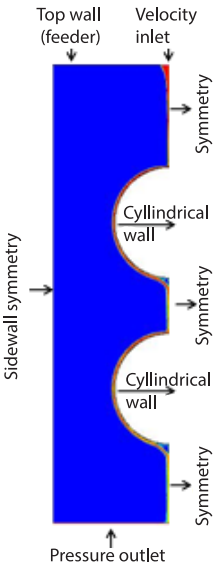

Figure 1. The CFD model

Assumptions

The assumptions made for the CFD analysis for all the three models are:

- Film flow is assumed to be laminar in the thermally developed region.
- Impingement of feed water on the top of the tube is in the form of sheet mode for a given saturation temperature.
- Gravitational forces are considered dominant than the inertial forces.
- Liquid film falls only in the direction of the gravitational forces.
- Evaporation occurs at the liquid-vapour interface.
- Liquid density is assumed to be constant.
- No scale formation is assumed.
- Non-condensable gas presence is not assumed.

Governing equations

The flow is governed by the Navier-Stokes equation. The continuity equation is given:

$$\frac{\partial \rho}{\partial t} + \nabla(\rho v) = 0 \tag{1}$$

The momentum equation in horizontal direction (x-axis) is given:

$$\frac{\partial u}{\partial t} + u\frac{\partial u}{\partial x} + v\frac{\partial u}{\partial y} = -\frac{1}{\rho}\frac{\partial p}{\partial x} + \vee\left(\frac{\partial^2 u}{\partial x^2} + \frac{\partial^2 u}{\partial y^2}\right) \tag{2}$$

The momentum equation in vertical direction (y-axis) is given:

$$\frac{\partial v}{\partial t} + u\frac{\partial v}{\partial x} + v\frac{\partial u}{\partial y} = -\frac{1}{\rho}\frac{\partial p}{\partial y} + \vee\left(\frac{\partial^2 v}{\partial x^2} + \frac{\partial^2 v}{\partial y^2}\right) + \mathrm{g} \tag{3}$$

The fluid energy equation is given:

$$\frac{\partial T_L}{\partial t} + u\frac{\partial T_L}{\partial x} + v\frac{\partial T_L}{\partial y} = \left[\alpha_L \frac{\partial^2 T_L}{\partial x^2}\right] + \left(\alpha_L \frac{\partial^2 T_L}{\partial y^2}\right) \tag{4}$$

Initial and boundary conditions

Table 1. Input parameters to the CFD models

Simulation	2-D
Solver	Pressure based, laminar, unsteady
Two-phase model	VOF
Primary phase	Air
Secondary phase	Water vapour and water
Gravitational acceleration	Downward in Y direction
Tube wall / Heat flux	Constant temperature / Flux
Volume of fraction for water	1
Volume of fraction for vapour	0
Pressure velocity coupling	PISO
Discretization pressure	PRESTO
Top boundary	Velocity inlet
Bottom side boundary	Pressure outlet
Side boundary	Symmetry
Wall boundary	Tube curvature

Physical models

A physical model employed in the current simulation studies is discussed.

Evaporation-condensation model

The evaporation-condensation model (liquid-vapour mass transfer) is governed by vapour transport equation [12, 13]:

$$\frac{\partial}{\partial t}(\alpha\rho_v) + \nabla(\alpha\rho_v V_v) = m_{l\to v} - m_{v\to l} \tag{5}$$

where ρ is the density, T_L – the liquid temperature, u – the x-component of water velocity, v – the y-component of water velocity, α_L – the thermal diffusivity, g – acceleration due to gravity in y-direction, v – the vapour phase, α – vapour volume fraction, ρ_v – vapour density, V_v – the vapour phase velocity, and $m_{l\to v}$ and $m_{v\to l}$ are the rate of mass transfer due to evaporation and condensation, respectively [kgs^{-1}m^{-3}].

The $m_{l\to v}$ and $m_{v\to l}$ are determined using the relations:

– If $T_L > T_s$ then

$$m_{l\to v} = \text{coeff}\alpha_L\rho_l\frac{T_L - T_s}{T_s} \tag{6}$$

– If $T_L < T_s$ then

$$m_{v\to l} = \text{coeff}\alpha_v\rho_v\frac{T_v - T_s}{T_s} \tag{7}$$

where coeff is coefficient of mass transfer determined by the following equation:

$$\text{coeff} = \frac{Cp_l T_s}{L_v} \tag{8}$$

where L_v [kJkg^{-1}] is the latent heat of evaporation and T_s – the saturation temperature. Using the eq. (9) the mass transfer coefficient (MTC) can be determined. Current analysis involves evaporation of liquid at the interface. Coefficient denotes the mass transfer intensity factor or relaxation time with unit [s^{-1}]. The value of coefficient is recommended to be such as to maintain the interfacial temperature reasonably close to the saturation temperature as well as to avoid divergence issues.

Meshing of the model

The GAMBIT software tool was used for modelling as well as meshing the 2-D domain of the geometry. Tri pave mesh was used in the present study. The region around the periphery of the tube was meshed carefully for capturing the details of the liquid-flow around the tubes and to precisely measure the water film thickness. A size function technique was also employed which ensures starting of mesh with fine size in the region closer to tube wall where flow of liquid is dominant and becomes coarse mesh in the region away from the tube wall. The size factor chosen is 0.05 mm with growth rate of 1.1 to a size limit of 1. The mesh model is shown in fig. 2.

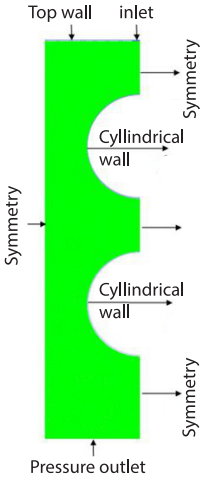

Figure 2. Meshing of CFD model

Solution methods

The PISO scheme

The PISO algorithm is nothing but the expansion of pressure implicit with splitting of operators. Issa [14] proposed this algorithm. This algorithm is chosen since it requires no iterations large time steps and a minimal computational effort.

Green-Gauss node based gradient

According to Mishriky and Walsh [15], the Green-Gauss node based (GGNB) method approximates the face value, Φ_f, as the average of the nodes enclosing the face:

$$\Phi_f = \frac{1}{N_{fv}} \sum_{j=1}^{N_{fv}} \Phi N_j \tag{9}$$

where N_{fv} is the number of nodes defining the face and ΦN_j – the nodal value at the j^{th} node, which in turns is determined as the weighted average of all the neighbouring cells using:

$$\Phi N_j = \frac{\sum_{i=1}^{n} \Phi_i w_i}{\sum_{i=1}^{n} w_i} \tag{10}$$

where n represents the number of neighbouring cells.

The PRESTO

Pressure staggering option is the expansion for PRESTO. Discrete continuity balance is used in this scheme about the face to compute the *staggered* (*i.e.*, face) pressure for a *staggered*' control volume. Generally in staggered arrangement, the pressure nodes are located at the centroid of grid cell and velocity nodes at the centre of the faces of the each cell in finite difference method and finite volume method. A staggered-grid scheme used for structured meshes follows similar procedure as suggested by Patankar [16].

First order upwind momentum

An upward wind scheme is nothing but a numerical discretization method for solving PDE of hyperbolic type. This scheme employs finite difference method to simulate numerically the direction in which flow field happens to obtain information such as velocity and pressure in the cell face. Courant *et al*. [17] proposed the upward wind scheme.

The CICSAM

The compressive interface capturing scheme for arbitrary meshes (CICSAM) is proposed by Ubbink [18]. According to him, it is the blend between the Hyper-C and the ULTIMATE-QUICKEST (UQ) schemes, with a blending factor of γ_f that in turn is based on the angle between the direction of motion and interface. This scheme is applicable for arbitrary meshes.

Convergence criteria

A convergence criterion of 10^{-3} is used for mass and 10^{-5} for momentum and energy residuals, respectively. Time step of 0.001 second is used in simulation.

Grid independence study

For the given model as shown in tab. 2 minimum cell counting grid size (0.05 mm) was chosen for the model studies which converge at a minimum computational time without losing solution accuracy.

Table 2. Grid independence study

Grid size [mm]	0.03	0.04	0.05
Liquid film thickness at $\theta = 90°$, m	0.000155	0.000159	0.000159

Results and discussions

Studies on the un-wetted area on the circular tubes at high wall super heat and low spray density

Heat flux and wall super heat on heat transfer coefficient

Effect of heat flux on the HTC is analyzed using CFD and results are compared with experimental values of Yang and Shen [19] for the same heat flux value as shown in fig. 3. An agreement up to 10% is observed between the results of CFD and experiments for the HTC. Figure 1 clearly indicates that as the heat flux increase, the HTC also increase correspondingly as a result of increase in wall superheat ($T_w - T_s$) due to rise in the surface temperature of the tube wall as shown in fig. 4, which indicates an increment in wall superheat as the heat flux increases. This in turn increases the amount of the heat transferred to liquid for a given liquid feed spray density (0.022 kg/ms) that obviously resulted in enhanced HTC value. The 20% deviation is observed between the CFD and experimental results for the superheat value ($T_w - T_s$) with respect to the heat flux as shown in fig. 4.

This deviation could be due to the fact that the Yang and Shen [19] conducted experiment by-passing steam inside tubes in order to heat and evaporate the liquid sprayed over the tubes. Due to latent heat of condensation, the steam condensed to form film on the inner wall surface of the tubes, which may exhibit thermal resistance in some portions of the tubes. This in turn would reduce the experimental value in comparison with CFD value and lead to deviation up to 20% maximum. On the other hand, previously discussed phenomenon is not considered in the CFD analysis. Each simulation is carried out with constant heat flux and resultant increase in superheat value is noted and compared with experimental results indicated in fig. 4. It is understood from the aforementioned comparative study that by increasing the heat flux, both the wall temperature and superheat increases. This would possibly create turbulence in the film of liquid-flowing over tubes because of reduced liquid viscosity and surface tension. This in turn led to increased HTC. It is also observed from fig. 3 that with the increase of the heat flux there observed a drop in the HTC value corresponding to the low spray density of 0.002 kg/ms. Formation of un-wetted surface on the tube wall at a spray density of 0.002 kg/ms at a wall super heat of 10 °C as indicated in fig. 5.

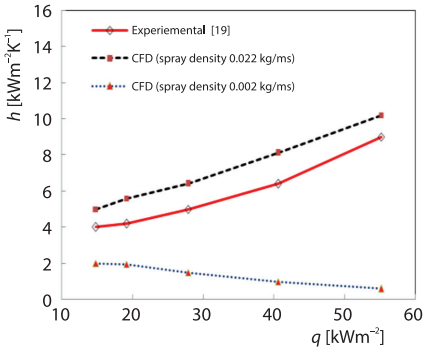

Figure 3. Effect of heat flux, q_{flux}, on average HTC [$Wm^{-2}K^{-1}$] at spray densities, Γ, of 0.022 and 0.002 kg/ms

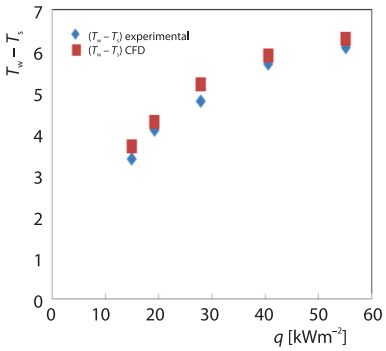

Figure 4. Effect of q_{flux} on wall super heat [K] at spray density, Γ, of 0.022 kg/ms

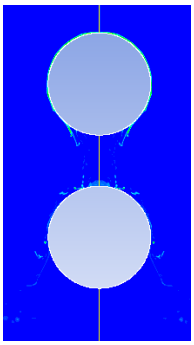

Figure 5. Contours of the film thickness [mm] around the tubes at 0.002 kg/ms

Effect of wall super heat on un-wetted area

In order to investigate the formation of un-wetted area on the tube surface and its influence on the HTC and mass transfer rate, a simulation studies have been carried out using a 14 mm outer diameter tube with input parameters obtained from the experiments conducted by Yang *et al*. [19]. The objective of the present study is to find out at what super heat temperature the dry patch forms on the tube surface with location for the given spray density. From the simulation contours of the liquid film thickness on the tube surface as shown in the figs. 6(a)-6(f), it is observed that no sign of un-wetted surfaces on the tube surface up to 6 °C wall super heat, but when the temperature of the wall heated up and wall super heat reaches 7 °C, a liquid vapour mixture starts developing between the liquid film and the tube surface close to the angle of around 20° from the top 0° angle and continues up to 165° angle at the bottom of the tube. It is also noted that the liquid film slides on these vapour mixture and seems to be not touching the tube surface on some portions of tube curvature and finally it leaves out the tube at bottom portion. This could be because of the formation of the vapour bubble within the liquid film near to the tube surface getting heated up to form bubble instantly due to high wall temperature. However, the present model used in this simulation could not able to predict the bubble formation but could predict by indicating that some phase transformation occurs near to the wall by showing change in volume of fraction from the liquid film to liquid vapour mixture around that region. When the super heat is not enough to develop liquid bubble on the tube surface, it would conduct heat with in the liquid film and increases its temperature gradually while film of liquid slides over the tube surface. Evaporation starts to happen in liquid vapour interface region. But from this simulation with increase in wall super heat with no change in the liquid film flow rate this phenomenon of liquid vapour mixture is observed between the tube surface and liquid film.

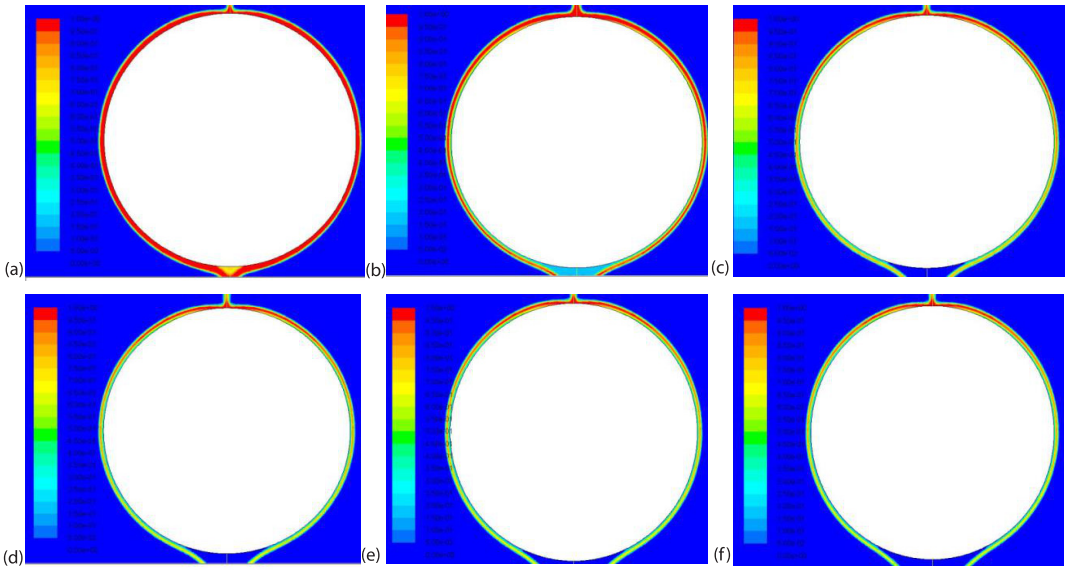

Figure 6. Contours of the film thickness [mm] around the tubes for circular tube at different wall super heat temperature, $T_w - T_s$, and at spray density, Γ, of 0.022 kg/ms; (a) $T_w - T_s = 6$ °C, (b) $T_w - T_s = 7$ °C, (c) $T_w - T_s = 8$ °C, (d) $T_w - T_s = 9$ °C, (e) $T_w - T_s = 10$ °C, and (f) $T_w - T_s = 11$ °C

It is observed from the fig. 6(a) that a liquid film flows on the surface of the curvature of the tube completely without any vapour liquid mixture between the liquid film and the hot tube surface corresponding to the wall super heat of 6 °C. However when the wall super heat temperature is increased to 7 °C as indicated in fig. 6(b), the liquid vapour mixture first time appears in the region of 20° angle and with further increase of wall super heat temperature up to 8-11 °C, the amount of liquid vapour mixture found to be increasing correspondingly as indicated in the figs. 6(c)-6(f), respectively. Also it is clearly visible from figs. 6(b)-6(f) that the bottom portion of the tube found to be not covered by the liquid film which resulted in the un-wetted surface at the bottom surface of the tube. The current simulation used evaporation-condensation model which could able to capture only the particle with temperature greater than the liquid temperature corresponding to saturation temperature of the evaporator. The contours of the mass transfer rate is shown in figs.7(a)-7(f) corresponding to the wall super heat

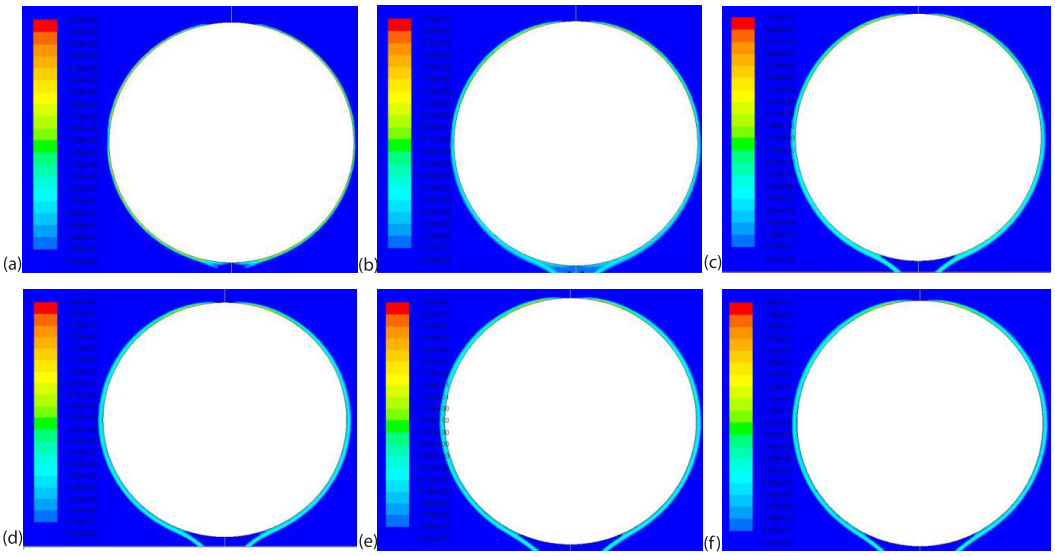

Figure 7. Contours of the mass transfer rate [kgm^{-3}s^{-1}] around the tubes for circular tube at different wall super heat temperature $T_w - T_s$, and at spray density, Γ, of 0.022 kg/ms; (a) $T_w - T_s = 6$ °C, (b) $T_w - T_s = 7$ °C, (c) $T_w - T_s = 8$ °C, (d) $T_w - T_s = 9$ °C, (e) $T_w - T_s = 10$ °C, and (f) $T_w - T_s = 11$ °C

of 6-11 °C, respectively. These figures clearly indicates that with the increase of the wall super heat there is a corresponding increment in the mass transfer rate or evaporation rate and after reaching certain wall super heat, the pattern of the curve show declining trend which indicates no further increment happens in the evaporation rate. The liquid film as it moves downwards its liquid film state gradually converted to the liquid vapour mixture state that lead to the formation of un-wetted surface at the bottom portion of the tube. This phenomenon attributed to the reduction in the average HTC of the tube for all the super heat wall temperatures except for

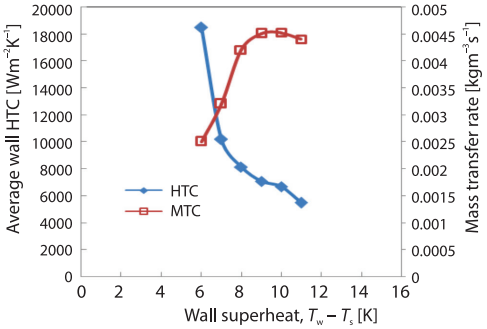

Figure 8. Effect of the wall super heat temp, $T_w - T_s$, on HTC [Wm^{-2}K^{-1}] and mass transfer rate [kgm^{-3}s^{-1}] for circular tube at spray density, Γ, of 0.022 kg/ms

6 °C as indicated in fig. 8. It is depicted in fig. 8 that with the increment of the wall super heat there observed a reduction in the HTC value from 18 kW/m^{2}K corresponding to super heat value of 6 °C to 6 kW/m^{2}K corresponding to the value of 11 °C. However, it is observed from the same fig. 8 that the MTC or evaporation rate is showing an increasing trend even though liquid vapour mixture forms between the liquid film and the tube outer surface as well as un-wetted area or dry patch formation at the bottom portion of the tube. This could be due to the elevated wall temperature which instantly heats up the liquid film to form vapour at the liquid film and tube surface interface which reflects boiling phenomenon where vapour bubbles nucleates within the liquid film on the heated wall surface.

Conclusion

The present CFD work investigated about the formation of un-wetted surface on the tube and its effect on the HTC and MTC of falling film evaporation. When the wall super heat increases above 6 K, the volume fraction mixture or phase change appears in between the liquid film and tube surface. This can be claimed as nucleate boiling, but the physical model used here is evaporation-condensation model, which could able to capture only the particle whose temperature is greater than or equal to the saturation temperature maintained around the tube outer diameter. This model could not able to capture the bubble formation. The threshold value to initiate nucleation or phase change to near tube happened to be at 6 K. As the wall super heat increases above 6 K, the HTC displayed declining trend could be due to formation of un-wetted area or dry out portion. But the MTC showed an increasing trend upto certain extent and then no further improvement is observed.

Nomenclature

A – heat transfer area of the tubes, [m^2]
C – constant for tube diameter
d – tube diameter, [m]
g – acceleration due to gravity, [ms^{-1}]
h_{wall} – wall HTC, [Wm^{-2}K^{-1}]
L – tube length, [m]
$m_{l\to v}$ – rate of mass transfer due to evaporation, [kgs^{-1}m^{-3}]
$m_{v\to l}$ – rate of mass transfer due condensation, [kgs^{-1}m^{-3}]
Pr – Prandtl number, ($=\mu_l Cp/k$)
q_{flux} – heat flux, [Wm^{-2}]
R – radius of the tube, [m]
Re – Reynolds number,($=\rho v d/\mu_l$)
T_s – saturation temperature, [°C]
T_w – wall temperature, [°C]
u – x-component of water velocity, [ms^{-1}]
V_v – vapour phase velocity, [ms^{-1}]
v – y-component of water velocity, [ms^{-1}]
v_l – vapour phase direction
w – width of jet, [m]

Greek symbols

α – vapour volume fraction
α_L – thermal diffusivity, [m^{2}s^{-1}]
Γ – liquid spray density, [kgm^{-1}s^{-1}]
θ – circumferential angle of tube, [°]
μ_l – dynamic viscosity, [Ns^{-1}m^{-2}]
ν – kinematic viscosity, [ms^{-2}]
ρ – density of fluid, [kgm^{-3}]
ρ_f – density of fluid, [kgm^{-3}]
ρ_g – density of gas, [kgm^{-3}]

Acronyms

HTC – heat transfer coefficient, [Wm^{-2}K^{-1}]
MED – multi effect distillation
MTC – mass transfer coefficient

References

[1] Asbik, M., *et al.*, Numerical Study of Boundary-Layer Transition in Flowing Film Evaporation on Horizontal Elliptical Cylinder, *Heat and Mass Transfer*, *48* (2005), 7, pp. 645-669
[2] Pu, L., *et al*., Effects of Tube Shape on Flow and Heat Transfer Characteristics in Falling Film Evaporation, *Applied Thermal Engineering*, *148* (2019), Feb., pp. 412-419
[3] Zhou, Y., *et al*., Numerical Simulation of Double-Phase Coupled Heat Transfer Process of Horizontal Tube Falling Film Evaporation, *Applied Thermal Engineering*, *118* (2017), C, pp. 33-40

[4] Christians, M., *et al*., Film Condensation of R-134a and R236fa – Part 1: Experimental Results and Predictive Correlation for Single-Row Condensation on Enhanced Tubes, *Heat Transfer Engineering*, *31* (2010), 10, pp. 799-808
[5] Tahir, F., *et al*., Review on CFD Analysis of Horizontal Falling Film Evaporators in Multi Effect Desalination Plants, *Desalination and Water Treatment*, *166* (2019), Oct., pp. 296-320
[6] Esquivel, J. F., *et al*., Hydrodynamic Analysis of the Falling Film Formation in Evaporators using CFD Simulations, *Food and BioProducts Processing*, *101* (2017), Jan., pp. 56-67
[7] Wang, B. X., *et al*., Experimental Study on the Dry out Heat Flux of Falling Film Liquid Film, *International Journal of Heat and Mass Transfer*, *43* (2000), 11, pp. 1897-1903
[8] Bohn, M. S., Davis, S. H., Thermocapillary Breakdown of Falling Films at High Reynolds Numbers, *International Journal of Heat and Mass Transfer*, *36* (1993), 7, pp. 1875-1881
[9] Zhiwei, T., *et al*., Experimental Study on Surface Wave and Film Breakdown of Faling Liquid Film Flow, *Heat and Mass Transfer*, *45* (2009), 6, pp. 673-677
[10] Yang, L., *et al*., Effect of the Dry out in Tube Bundles on the Heat Transfer Performance of Falling Film Evaporators, *Procedia Engineering*, *205* (2017), Dec., pp. 2176-2183
[11] Li, H., *et al.*, Numerical Simulation for Falling Film Flow Characteristics of Refrigerant on the Smooth and Structured Surfaces, *Journal of Engineering Thermophysics*, *27* (2018), Mar., pp. 1-19
[12] Lee, W., *A Pressure Iteration Scheme for Two-Phase Flow Modelling, Multi-Transport Fundamentals, Reactor Safety, Applications*, (ed. T. N. Veziraglu), Hemisphere Publishing, Washington, USA, 1980, Vol. 1, pp. 407-431
[13] Balaji, D., *et al.*, Numerical Investigation on the Effect of Tube Geometry and Feeder Height on the Heat Transfer Performance of Horizontal Tube Falling Film Evaporation, *Journal of Heat Transfer*, *141* (2019), 11, pp. 111502-111516
[14] Issa, R. I., *et al*., The Computation of Compressible and Incompressible Recirculating Flows by a Non-Iterative Implicit Scheme, *Journal of Computational Physics*, *62* (1986), 1, pp. 66-82
[15] Mishriky, F., *et al*., Towards Understanding the Influence of Gradient Reconstruction Methods on Unstructured Flow Simulations, *Transactions-Canadian Society for Mechanical Engineering*, *41* (2017), 2, pp. 169-179
[16] Patankar, S. V., *Numerical Heat Transfer and Fluid-Flow*, McGraw-Hill, New York, USA, 1980
[17] Courent, R., *et al*., On the Solution of Non-Linear Hyperbolic Differential Equations by Finite Differences, *Communications on Pure and Applied Mathematics*, *5* (1952), 3, pp. 243-255
[18] Ubbink, O., Numerical Prediction of Two-Phase Fluid Systems with Sharp Interfaces, Ph. D. thesis, University of London, London, UK, 1997
[19] Yang, L., *et al*., Experimental Study of Falling Film Evaporation Heat Transfer Outside Tubes, *Desalination*, *220* (2008), 1, pp. 654-660

Paper submitted: April 14, 2020
Paper revised: October 5, 2020
Paper accepted: November 22, 2020